Sml1p Is a Dimer in Solution: Characterization of Denaturation and Renaturation of Recombinant Sml1p[†]

Vibha Gupta,[⊥] Cynthia B. Peterson,[⊥,#] Lezlee T. Dice,[⊥] Tomoaki Uchiki,[‡] Joseph Racca,[⊥] Jun-tao Guo,[§] Ying-Xu,[§,#] Robert Hettich,[‡,#] Xiaolan Zhao,[▽,||] Rodney Rothstein,[▽] and Chris G. Dealwis*[,⊥,#]

Department of Biochemistry and Cellular and Molecular Biology, University of Tennessee, Knoxville, Tennessee 37996, Genome Science and Technology Graduate School, University of Tennessee-Oak Ridge National Laboratory, Protein Informatics Group, Life Sciences Division and Computer Sciences and Mathematics Division, Oak Ridge National Laboratory, Oak Ridge, Tennessee 37830-6480, Chemical Sciences Division, Oak Ridge National Laboratory, Oak Ridge, Tennessee 37831, and Department of Genetics and Development, Columbia University, College of Physicians & Surgeons, New York, New York 10032

Received December 3, 2003; Revised Manuscript Received April 27, 2004

ABSTRACT: Sml1p is a small 104-amino acid protein from *Saccharomyces cerevisiae* that binds to the large subunit (Rnr1p) of the ribonucleotide reductase complex (RNR) and inhibits its activity. During DNA damage, S phase, or both, RNR activity must be tightly regulated, since failure to control the cellular level of dNTP pools may lead to genetic abnormalities, such as genome rearrangements, or even cell death. Structural characterization of Sml1p is an important step in understanding the regulation of RNR. Until now the oligomeric state of Sml1p was unknown. Mass spectrometric analysis of wild-type Sml1p revealed an intermolecular disulfide bond involving the cysteine residue at position 14 of the primary sequence. To determine whether disulfide bonding is essential for Sml1p oligomerization, we mutated the Cys14 to serine. Sedimentation equilibrium measurements in the analytical ultracentrifuge show that both wild-type and C14S Sml1p exist as dimers in solution, indicating that the dimerization is not a result of a disulfide bond. Further studies of several truncated Sml1p mutants revealed that the N-terminal 8−20 residues are responsible for dimerization. Unfolding/refolding studies of wild-type and C14S Sml1p reveal that both proteins refold reversibly and have almost identical unfolding/refolding profiles. It appears that Sml1p is a two-domain protein where the N-terminus is responsible for dimerization and the C-terminus for binding and inhibiting Rnr1p activity.

Eukaryotic cells have evolved multiple strategies to tolerate genomic damage. These include DNA repair systems that remove or bypass potential mutagenic DNA lesions (*1*, *2*) and cell cycle delays at multiple transition points after exposure to DNA damaging agents (*3*−*5*). Weinert and Hartwell (*2*) first observed the control of these delays in budding yeast and called them DNA checkpoints. Defects in checkpoint regulation can lead to genomic instability, which is one of the hallmarks of cancer cells (*3*, *6*).

In *Saccharomyces cerevisiae*, the Mec1p and Rad53p proteins are required for G1, S, and G2 cell cycle checkpoint pathways (*7*). During DNA damage or DNA replication, these proteins are required to arrest cell cycle progression. Simultaneously, these checkpoint pathway proteins also induce transcription of ribonucleotide reductase (RNR),[1] an enzyme responsible for catalyzing the rate-limiting step in dNTP synthesis (*8*−*10*). During DNA synthesis and repair, the activity of RNR is tightly regulated by the Mec1/Rad53/Dun1 kinase cascade (*8*). For *S. cerevisiae* until recently, only three RNR regulatory mechanisms were known: (1) allosteric regulation (*9*, *10*), (2) transcriptional regulation of RNR genes during the cell cycle (*11*−*15*), and (3) regulation through nuclear localization of Rnr2p and Rnr4p (*16*). Another mode of regulation involving a protein inhibitor of RNR, designated Sml1p, was recently discovered in yeast

[†] This work is supported by the National Institute of Health, Grant Numbers 1R01CA100827-01 and GM50237. T.U. acknowledges financial support from the Genome Science and Technology Graduate School, University of Tennessee−Oak Ridge. R.R. is supported by NIH Grant GM50237.

* Corresponding author. Mailing address: Department of Biochemistry and Cellular and Molecular Biology, M407, Walters Life Science Building, University of Tennessee, Knoxville, TN 37996. Phone: (865)-974-4088. E-mail: cdealwis@utk.edu.

[⊥] University of Tennessee.

[#] Members of the Center for Excellence in Structural Biology at the University of Tennessee − Knoxville.

[‡] University of Tennessee-Oak Ridge National Laboratory.

[§] Mathematics Division, Oak Ridge National Laboratory.

[‡] Chemical Sciences Division, Oak Ridge National Laboratory.

[▽] Columbia University, College of Physicians & Surgeons.

[||] Present address: The Rockefeller University, 1230 York Avenue, New York, NY 10021.

[1] Abbreviations: RNR, ribonucleotide reductase; Rnr1p, large subunit of yeast ribonucleotide reductase (p is appended to a protein name to indicate that it originates in *S. cerevisiae*); Sml1p, suppressor of *mec1* lethality; WT, wild-type; C14S, cysteine at position 14 mutated to serine; Sml1p-histag, Sml1p with a His tag at the C-terminus; Δ38Sml1p, Sml1p mutant with first 38 residues truncated; GST, glutathione S-transferase; CD, circular dichroism; DTT, dithiothreitol; GdnHCl, guanidine hydrochloride; PAGE, polyacrylamide gel electrophoresis; IPTG, isopropyl β-D-thiogalactopyranoside; EDTA, ethylenediamine-tetraacetic acid; PMSF, phenylmethylsulphonyl fluoride.

10.1021/bi0361721 CCC: $27.50
Published on Web 06/11/2004

(*45*). Sml1p specifically binds to the large subunit of yeast RNR (Rnr1p) and efficiently inhibits RNR activity when DNA synthesis is not required.

Since *mec1*Δ or *rad53*Δ yeast strains are unable to grow in the presence of Sml1p, their lethality can be suppressed by expression of a mutated Sml1p that is unable to bind Rnr1p (*17*−*19*). Furthermore, *sml1* affects various cellular processes similarly to overexpression of Rnr1p. Consistent with these observations, the levels of intracellular dNTPs are increased in a *sml1*Δ yeast strain compared to the wild-type strain, suggesting that Sml1p is a negative regulator of dNTP synthesis. Therefore, in addition to regulation of RNR activity at the transcriptional level (*20*), the RNR activity is also regulated by its inhibitor, Sml1p, (*17*) in a Mec1- and Rad53-dependent manner (*21*).

Zhao and co-workers demonstrated that Sml1p is a new substrate of the Mec1/Rad53 kinase cascade (*21*). Accordingly, a model for Mec1 and Rad53 function in RNR regulation during DNA damage and replication has been suggested. After DNA damage or at S phase, the Mec1/Rad53/Dun1 kinase cascade is activated, leading to phosphorylation of Sml1p by Dun1p (*8*, *22*). The phosphorylated Sml1p is immediately removed. Zhao and co-workers (*21*) have proposed that free Sml1p is in equilibrium with the Sml1p−Rnr1p complex and the degradation of free Sml1p drives the equilibrium from the inactive Sml1p−Rnr1p complex to the active form of RNR. However, as of yet it is not certain whether both the free and Rnr1p-bound Sml1p might be subjected to phosphorylation. These authors also show that the decrease in Sml1p levels during S phase and after DNA damage is due to posttranscriptional regulation and occurs in tandem with phosphorylation of Sml1p.

Although Sml1p has been characterized in vivo using genetic and molecular assays, there is very little biochemical or structural data available on the protein. Despite the keen interest in structure−function relationships of Rnr1p−Sml1p, there are no three-dimensional structures available for the Sml1p−Rnr1p complex or for free Rnr1p or Sml1p. However, some secondary structural components have been assigned by a nuclear magnetic resonance (NMR) study, which has observed two helices of Sml1p (*23*).

The oligomeric state of native Sml1p is not known. While characterizing this protein by electrospray mass spectrometry, we observed that Sml1p−histag readily forms intermolecular disulfide bonds involving the only cysteine residue, which is found at position 14 in the primary structure of this protein (*24*). To further investigate this oligomerization, we mutated Cys14 to serine (C14S). In this study, we employ a variety of biophysical techniques to characterize the self-association and folding of both variants of Sml1p. The unfolding/refolding studies reported here provide insights into the domain structure of Sml1p.

MATERIALS AND METHODS

Chromatography was performed on a BioLogic HR chromatography system from BioRad. The Superdex-G75 Column and Glutathione Sepharose 4 Fast Flow resin were procured from Amersham Pharmacia Biotech. A low molecular weight gel filtration calibration kit was also purchased from Amersham Pharmacia. Protease inhibitor cocktail tablets (Complete) were obtained from Roche Diagnostics. Coomassie Plus protein assay reagent was purchased from Pierce. Ultrapure acrylamide and molecular biology grade DTT were products of Fisher Biotech. Analytical grade IPTG was purchased from Alexis Chemicals. All other chemicals were reagent grade and were purchased from common sources.

The cloning of wild-type (WT) SML1 has been described in Zhao et al. (*45*). To construct an expression plasmid that contains *C14S-sml1*, the WT expression plasmid was mutated using the QuickChange site-directed mutagenesis kit (Stratagene, La Jolla, CA). The forward primer used for C14S was 5′-CGCTCAAAATCGCTCCCAACAACAACAAGCC-3′ and the corresponding reverse primer was 5′-GGCTTGT-TGTTGTTGGGAGCGATTTTGAGCG-3′ (the mutation sites are underlined) for the PCR reaction. Plasmid DNA was purified from isolated colonies that appeared after transformation, and the mutation was confirmed by DNA sequencing of plasmid DNA at the Molecular Biology Resource Facility, University of Tennessee, Knoxville.

The Δ8Sml1p, Δ20Sml1p and Δ38Sml1p were expressed from a pGEX vector containing glutathione transferase as a N-terminal fusion protein (Amersham Pharmacia Biotech) that had already been modified by inserting a human rhinovirus 3C protease (*25*) site between GST and the gene of interest. The insert was amplified by PCR using WT SML1 vector as a template. The three respective forward primers, which introduced a *Bam*HI site (5′GCTGCTG-GATCCCAAAATCGCTGCCAACAA-3′, 5′ GCTGCTG-GATCCTCCACATTGCGTACCGTG-3′, and 5′-GCTGCTG-GATCCATGGCTGAGGTTCCTATG-3′), and the single reverse primer, which introduced an *Eco*RI restriction site (5′-CTAAATGAATTCTCACTATTAGAAGTCCATTTC-CTC-3′), were synthesized by Integrated DNA Technologies Inc. PCR was carried out in 50 μL volume with 50 ng of forward and reverse primers, 25 ng of template, 2 mM $MgCl_2$, 0.2 mM dNTP mix, Taq buffer, and 1 μL of Taq polymerase (5U/μL). The amplified fragments and modified pGEX vector both were cleaved with *Bam*HI and *Eco*RI restriction enzymes. The insert was ligated into the dephosphorylated vector by overnight incubation at 15 °C with T4 DNA ligase (Fisher). DNA sequencing of the isolated construct confirmed the success of our cloning.

The WT or C14S Sml1p proteins were expressed and purified as described in ref *22*. The final yield of purified protein was ∼5 mg per liter of culture. For growth and expression of the Δ8Sml1p, Δ20Sml1p, and Δ38Sml1p in BL21(DE3)plysS *Escherichia coli* cells, we adopted the same procedure used for the WT Sml1p. For purification, the cell pellet was resuspended in 10 mL of lysis buffer optimized for glutathione sepharose resin [140 mM NaCl, 2.7 mM KCl, 10 mM Na_2HPO_4, 10% glycerol (pH 7.3), 10 mM DTT, 1 mM PMSF, and Complete protease inhibitor cocktail]. Cells were lysed in the manner described above for the full-length Sml1p. The lysate was incubated with 2 mL of resin at 4 °C for 2 h followed by washing the resin with 15−20 column volumes of lysis buffer. The Δ38Sml1p was freed from the GST fusion protein by equilibrating with 5 column volumes of 3C protease cleavage buffer [50 mM Tris, 150 mM NaCl, 10 mM EDTA (pH 8.0), and 1 mM DTT], followed by incubation with 3C protease (20 μg) for 1 h at room temperature. The cleaved truncated Δ8Sml1p, Δ20Sml1p, and Δ38Sml1p proteins were further purified on a Superdex-

G75 size-exclusion column. Approximately 5 mg of pure protein could be recovered from 1 L of culture with the above protocol.

A HiLoad 16/60 Superdex-G75 column from Amersham Biosciences was used at 4 °C for size-exclusion chromatography. The column was preequilibrated with buffer A (20 mM Tris-HCl (pH 7.5), 120 mM NaCl, 5 mM $MgCl_2$), and 2 mL samples containing 6−10 mg of protein were run at a flow rate of 1 mL/min. The absorbance of the column eluate was monitored at 280 nm, and fractions of 500 μL were collected. The molecular weight (MW) of the eluted protein was estimated by means of a calibration curve prepared using elution times measured for protein standards purchased from Amersham Biosciences. The standards used for the calibration were ribonuclease A, chymotrypsinogen, ovalbumin, and albumin, corresponding to 13.7, 25, 43, and 67 kDa molecular mass, respectively. K_{av} [(elution volume − void volume)/(column volume − void volume)] was plotted against −log(MW) for the standards curve. The respective purified fractions of WT and C14S Sml1p were loaded onto the Superdex-G75 column to determine the elution profiles of the pure protein.

Automatic Edman degradation was carried out at the Microchemical Facility of Emory University on an Applied Biosystems 477A pulsed-liquid sequencer in-line with an Applied Biosystems 120A PTH analyzer. Mass spectrometry measurements were acquired with an IonSpec (Irvine, CA) 9.4-Tesla HiRes electrospray Fourier transform ion cyclotron resonance mass spectrometer (ES-FTICR-MS), as described previously for the Sml1p-histag species (*24*). Protein concentrations were determined by a Bradford-based assay using Coomassie Plus protein assay reagent.

Equilibrium analytical ultracentrifugation was performed on an Optima XL-I analytical ultracentrifuge from Beckman Coulter as previously described (*26*). Sedimentation equilibrium experiments were performed with protein concentrations ranging from 0.2 to 1 mg/ml in buffer A with or without GdnHCl. Standard double-sector 12-mm Epon charcoal-filled cells with quartz windows were used in either an AN50Ti eight-hole rotor or AN60Ti four-hole rotor. Absorbance optics were used to follow the concentration gradient during the approach of the sample to equilibrium at 25 000−45 000 rpm by taking autoscans at 2 or 4 h intervals. Data were collected after equilibrium had been established. At equilibrium, the distribution of a single, homogeneous species within the ultracentrifuge cell is given by the equations

$$c_r = c_m \exp(\sigma) + \text{base} \quad (1)$$

$$\sigma = M(1 - \bar{\nu}\rho)\omega^2(r^2 - r_m^2)/(2RT) \quad (2)$$

in which c_r and c_m are the concentrations of the protein at radial position, r, and at a reference position, r_m (i.e., the meniscus), respectively. M is the molecular weight of the protein, $\bar{\nu}$ is the partial specific volume of the protein, ω is the angular velocity, ρ is the solvent density, R is the gas constant, and T is the absolute temperature (K). The "base" term is a constant that corrects for nonsedimenting baseline absorbance. The partial specific volume for Sml1p was calculated as 0.7106 (at 20 °C) from its amino acid composition using the program SEDNTRP written by Dr. John Philo, Alliance Protein Laboratories, Thousand Oaks, California. Solvent density, ρ, was estimated to be 1.004 for buffer A; the densities of guanidine solutions and partial specific volume for Sml1p at various GdnHCl concentrations were calculated according to Kawahara and Tanford (*27*) using SEDNTRP. For the analysis of samples containing multiple sedimenting species, the concentration distribution can be written as the sum of the distributions for the individual species, i, as

$$c_r = \sum c_{m,i} \exp(\sigma_i) + \text{base} \quad (3)$$

Models for monomer/dimer association defined by the equilibrium constant, K_a, and indefinite association (monomer/n-mer) were also evaluated. Analyses on single data sets and global analyses were performed using nonlinear least-squares methods with the program SEDPHAT, written by Dr. Peter Schuck at the National Institutes of Health (*28*).

CD spectra were obtained on an AVIV-2-2 circular dichroism spectrometer (AVIV Instruments, Lakewood, NJ) at 25 °C using a quartz cell with either 0.1 cm path length for 20 μM samples or 1 cm path length for 2 μM samples. All measurements were recorded with 1 nm bandwidth, and multiple accumulations were averaged for each sample. Contributions to the signal by the buffer were subtracted. Ellipticity in millidegrees was converted to molar ellipticity (ME) using the formula

$$\text{ME} = \text{millidegrees}/(\text{no. of residues} \times \text{conc} \times \text{cell length (cm)} \times 10) \quad (4)$$

The CD data were deconvoluted using the CDNN CD Spectra Deconvolution Program (version 2.1) obtained from the website http://bioinformatik.biochemtech.uni-halle.de/cdnn/.

GdnHCl- or urea-induced unfolding was monitored with both CD and fluorescence. Samples in varying concentrations of denaturant were incubated for 12 h at 4 °C. A 10-fold dilution of the unfolded samples with buffer, allowing each sample to reequilibrate at lower GdnHCl concentrations for 24 h, established the reversibility of the process.

The secondary structure of yeast Sml1p was predicted using PSIPRED V2.3, which has an average prediction accuracy of 75% for water-soluble proteins (*29*). Fold recognition and sequence−structure alignment were performed using the programs PROSPECT (*30*, *31*) and FUGUE (*32*). Models with high scores for the entire Sml1p protein sequence were generated using another template-based program, Rosetta/I-sites (*33*). Top models that were consistent with experimental data were selected as templates for constructing the intact structural model of Sml1p, using MODELLER (*34*). MODELLER provides the option of merging structures of protein sequence segments based on their overlapping regions. To check the stereochemical quality of the Sml1p model, PROCHECK was used to generate a number of plots including a Ramachandran plot (*35*). The structural models were visually inspected using Rasmol (*36*).

RESULTS

The identity of the recombinant protein was confirmed as follows: N-terminal sequencing was performed by automatic

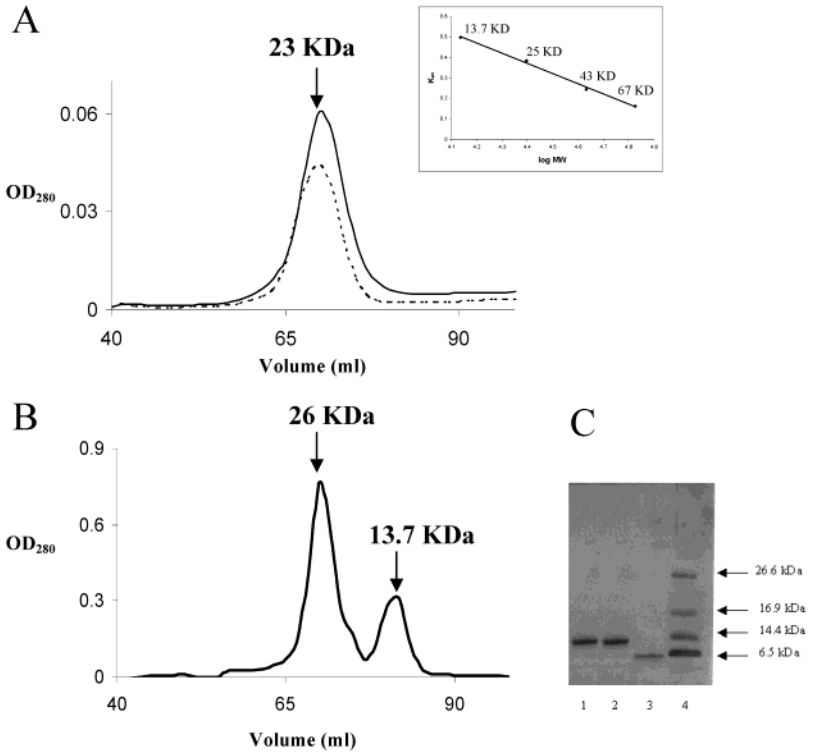

FIGURE 1: Size-exclusion chromatography. The lysate of WT or C14S Sml1p was precipitated by 25% ammonium sulfate, resuspended in 2 mL of buffer A, and loaded on 16/60 Superdex-G75 column. The purified fractions were loaded again on to the Superdex-G75 column. Panel A shows the elution profile beyond the void volume (40 mL) of the column for WT Sml1p (—) and C14S (···). The ability of the columns to resolve Sml1p monomers (11.9 kDa) from trimers (33.3 kDa) was tested by injecting a mixture of carbonic anhydrase (29 kDa) and Rnase A (13 kDa), using the same above buffer. Panel B shows the chromatograph of the mixture in solid lines. The two peaks are clearly resolved from each other where the highest points of the peaks correspond to 26 kDa (peak 1 from left to right) and 13.34 kDa for (peak 2 from left to right), respectively. Panel C displays the 15% SDS−PAGE: (lane 1) WT Sml1p; (lane 2) C14S Sml1p; (lane 3) Δ38Sml1p; (lane 4) molecular mass marker. In the inset, proteins with known molecular masses were used for the calibration curve representing log MW (molecular weight) as a function of the distribution coefficient K_{av}.

Edman degradation, in which the first nine cycles yielded the sequence G-S-M-Q-N-S-Q-D-Y. Other than glycine and serine, the rest of this sequence is identical to the native Sml1p sequence (Figure 8a). The first two residues are introduced as a result of cloning into the pWJ750-2 expression vector. Mass spectrometry of the proteins yielded a molecular mass of 11 978 Da and 11 962 Da, in accord with that calculated from the sequence of WT Sml1p (11 978 Da) and C14S Sml1p (11 962 Da), respectively. In both cases, the extra two residues at the N terminus of the protein were taken into account.

Purification of recombinant Sml1p is achieved in three steps. The first two steps involving ultracentrifugation and ammonium sulfate fractionation are similar to those reported by Chabes et al. (*17*). The third step of ultrafiltration, through Ultrafree-MC Millipore 30 000 NMWL filter units in their protocol, has been replaced in our work by size-exclusion chromatography using a Superdex-G75 sizing column. For WT Sml1p, 5 mM DTT was used in the column buffer, whereas purification of C14S mutant was performed without any DTT in the buffer. Figure 1, panel A, shows results from prepurified Sml1p run over the Superdex-G75 column, along with a gel demonstrating the purity of the protein after size-exclusion (see panel C). The elution volumes for several protein standards were used to calibrate the column, as shown in the inset. The resolving capacity of the column is demonstrated in panel B, which shows the elution profile for a mixture of two of the protein standards with individual molecular weights of 13 000 and 29 000 Da. As shown in panel A, the wild-type Sml1p protein elutes as a fairly symmetrical peak, with an elution position intermediate between the two proteins shown in panel B corresponding to a calculated molecular weight of approximately 23 000 Da.

The gel filtration results indicated that Sml1p associates to a higher-order oligomer with a molecular weight indicative of a dimer. Since molecular weight estimates from size-exclusion chromatography can be skewed for nonspherical proteins, we pursued more definitive measurements of the molecular weight for Sml1p using analytical ultracentrifugation. Sedimentation equilibrium analyses are based on a radial distribution of a macromolecule that is a strict function of mass and independent of shape (*37*) and therefore are optimal for accurately determining molecular weights. Varying concentrations of Sml1p from 0.2 to 1 mg/mL were evaluated by sedimentation equilibrium at variable rotor speeds. A representative data set is shown in Figure 2, and results are summarized in Table 1. For both wild-type and the C14S mutant forms of Sml1p, results from sedimentation equilibrium analyses yield a molecular weight that is most consistent with a dimer.

Figure 2 shows fits of the data (shown in the solid squares) to two different models. Panel A shows a fit to a single species, a model that was satisfactory for both forms of Sml1p under a variety of conditions (Table 1). Results from five to six data sets give average (mean + SD) values for the molecular weight from the single-species fits of 22 830 for wild-type Sml1p and 21 180 for the C14S mutant Sml1p.

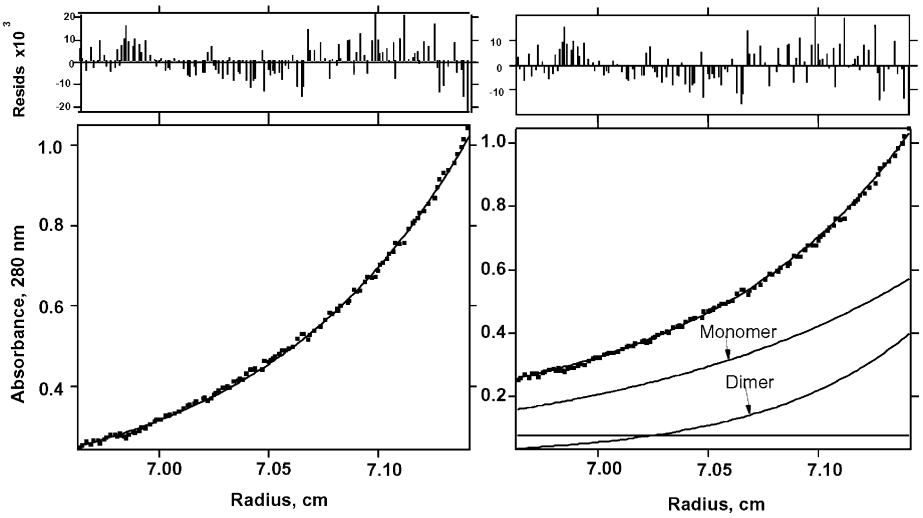

FIGURE 2: Equilibrium analytical centrifugation of C14S Sml1p. Data are shown in the solid squares, with the smooth curves in each panel representing nonlinear fits to the data according to their different models. In each of the fits, residuals are shown in the upper panel. Panel A shows a fit to a single species, a model that was satisfactory for both forms of Sml1p under a variety of conditions (Table 1). Panel B shows a fit of the data for the monomer/dimer model.

Table 1: Molecular Weight Determination for Wild-Type and C14S Sml1p Using Sedimentation Equilibrium Measurements

Sml1	conc (mg/mL)	speed (rpm)	temp (°C)	calcd MW[a]	χ^2 [b]	avg ± SD	global fit	local RMSD[e]
WT	0.8	25 000	4	25 300	0.057	22 000 ± 3100	24 300[c]	0.018
		30 000	4	19 700	0.029			0.0026
	0.6	25 000	4	25 000	0.022			0.012
		30 000	4	22 000	0.012			0.017
	0.2	25 000	4	18 200	0.005			0.009
C14S	1.0	25 000	4	19 800	0.013	21 300 ± 2200	22 200[d]	0.021
	0.85	25 000	4	21 800	0.017			0.017
	0.8	25 000	4	25 400	0.1			0.062
	0.8	25 000	4	19 200	0.02			0.014
	0.5	25 000	4	21 200	0.04			0.032
	0.2	25 000	4	20 100	0.008			0.009
	0.5	25 000	30	22 400	0.015			0.018

[a] Molecular weights were calculated from single-species model. [b] χ^2 values were calculated for the individual fits as $\sum_n((\text{residuals})_{\text{obsd}} - (\text{residuals})_{\text{exptd}})^2/(\text{residuals})_{\text{exptd}}$ expressed as a variance by dividing by $n - n' - 1$; n is the number of data points, and n' is the number of parameters being determined in the analysis. [c] A global fit of all data gave a value of 24 300 for WT Sml1 with a reduced χ^2 of 1.3. Reduced χ^2 is defined as: $x_2 = 1/N_e\sum_e 1/N_i^{(e)}\sum_i[(\text{data}_i^{(e)} - \text{model}_i^{(e)})/\delta^{(e)}]^2$ with a perfect fit getting a value of 1. In this equation, N_e = number of experiments, $Ni^{(e)}$ = number of data points for a specific experiment, and $\delta^{(e)}$ is the estimated measurement error in the experiment. [d] A global fit of all data for the C14S mutant form of Sml1 gave a value of 22 200 with a reduced χ^2 of 2.5. [e] RMSD values are given for each "local" data set, as calculated in the global analysis.

Note that the calculated molecular weight is not affected by the presence of reducing agents in the buffer, indicating that intermolecular disulfide bonding is not required to maintain the dimeric state of the protein. Panel B shows a fit for this particular data set to a monomer/dimer model, respectively. Not surprisingly, the monomer/dimer model fits the data well with a prominent dimeric form of Sml1p and small amount of monomer in the mixture. For the data sets analyzed, the quality of the monomer/dimer fit is comparable with the single-species fit with residuals and a χ^2 value that are virtually indistinguishable. Fits were also evaluated using a monomer/*n*-mer model, in which the known molecular weight of the monomer is included in the fit with a floating parameter, *n*, corresponding to oligomerization state. For this particular data set, *n* was close to 3, although fits to all of the data sets analyzed varied with *n* values between 2 and 5. In any case, when higher-order species exceeding dimers are considered in the fits, the association constants predict a majority of monomer and a much smaller amount of oligomer.

The unlikely possibility that Sml1p exists as a mixture of monomer and higher-order oligomers cannot be altogether excluded from the equilibrium sedimentation analyses alone. However, a global analysis of all the ultracentrifugation data on both wild-type and mutant forms of the protein yielded average molecular weights indicative of a dimer (Table 1). Also, a dimeric form of the protein is more consistent with gel filtration analysis on the protein, shown in Figure 1. A monomer/oligomer mixture of Sml1p should give a broad elution profile with the two species resolved by chromatography, if the species are in a slowly exchanging equilibrium. This is not observed with Sml1p (Figure 1A). Indeed, if a monomer/oligomer equilibrium were in more rapid exchange, the peaks could merge and appear as one boundary in gel filtration. However, the ultracentrifugation analyses using models considering higher-order (monomer/*n*-mer) association indicate that such mixtures would be dominated by monomers, so a merged peak would be expected to elute in gel filtration at an elution position closer to that expected for the monomer. Taken together, the data most strongly

Table 2: Molecular Weights of Truncated Forms of Sml1p Determined from Sedimentation Equilibrium Ultracentrifugation

protein	MW[a]	χ^2
Δ8Sml1p	21700	0.l2
Δ20sml1p	9600	0.033
Δ38Sml1p	7700	0.024

[a] Molecular weights calculated for a single-species fit

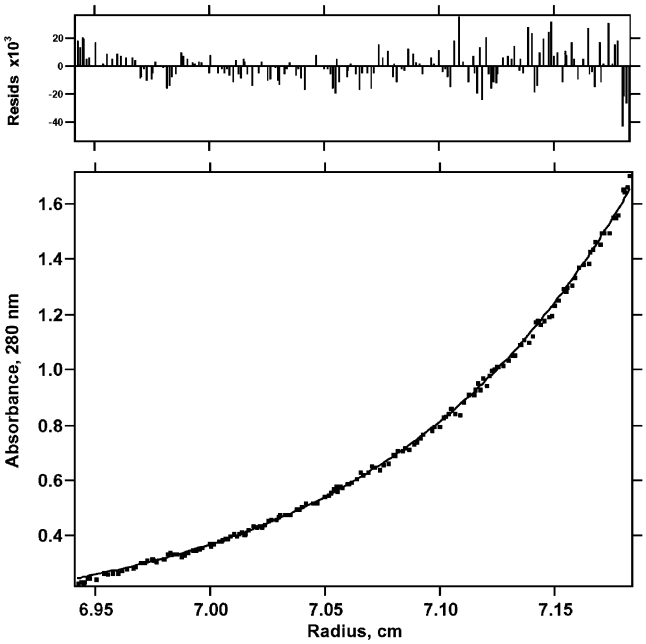

FIGURE 3: Equilibrium analytical centrifugation of Δ38Sml1p. This figure shows the radial distribution of absorbance in the centrifuge cell at equilibrium at 35 000 rpm for Δ38Sml1p at a concentration of 0.8 mg/ml in 20 mM Tris (pH 7.5), 120 mM NaCl, 5 mM $MgCl_2$. The solid line through the data represents the fit to a single species of molecular weight corresponding to 7670 Da. The residuals for the fit are shown in the upper panel.

argue for a dimeric state. Results from a single sedimentation equilibrium experiment conducted at 30 °C, which is the physiologic temperature for *S. cerevisiae*, with C14S Sml1p agreed with the above results from experiments conducted at 4 °C (Table 1).

To test which regions of Sml1p were involved in dimerization, we engineered three mutant forms of Sml1p with the N-terminal 8, 20, and 38 residues deleted. All these mutants are known to be active forms of Sml1p and inhibit activity of Rnr1p as strongly as WT Sml1p (*23*). The sedimentation equilibrium studies of Δ8Sml1p yield a single distribution with a molecular weight of 24 700 Da that is still a dimer (Table 2). However, the Δ20Sml1p and Δ38Sml1p mutants show single distributions that yield molecular weights of 9600 and 7670 Da, respectively, suggesting that the two truncated proteins are monomers in solution (Figure 3, Table 2). The observation that Δ20Sml1p is a monomer while Δ8Sml1p is a dimer argues that the dimerization domain must be found between the N-terminal residues 8 and 20.

Circular dichroism spectra of WT Sml1p and C14S Sml1p are similar (Figure 4). Deconvolution of each spectrum indicates the presence of about 20% α-helical structure, 28% β-sheet, and about 52% random coil for both WT and C14S Sml1p. These observations indicate that Sml1p is loosely

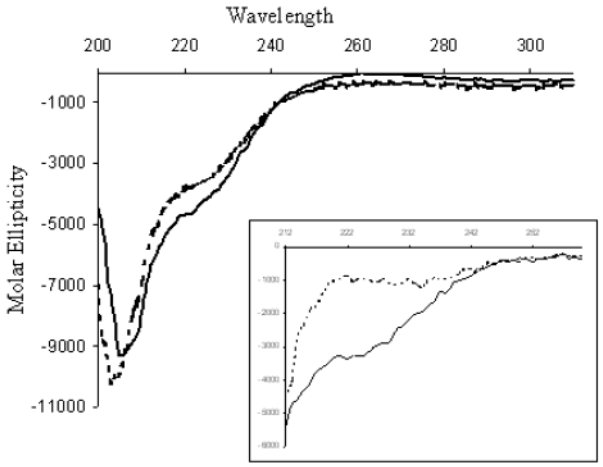

FIGURE 4: CD spectra of Sml1p. Circular dichroism spectra of WT (solid line) and C14S Sml1p (dashed line) were measured in buffer A using 35 μM protein concentration. In the inset, spectra for native WT Sml1p (solid line) in buffer A and denatured WT Sml1p in 4.8 M GdnHCl (dotted line) are shown for comparison.

folded in solution. We also observe the loss of negative ellipticity in 222 nm region for WT Sml1p versus denatured Sml1p in 6 M GdnHCl (Figure 4). This indicates the expected loss of secondary structure upon chemical denaturation.

This loss of negative ellipticity provided a convenient method to monitor unfolding and refolding of Sml1p in the presence of chemical denaturants. Denaturation of WT and C14S Sml1p as a function of either GdnHCl (Figure 5A) or urea (Figure 5B) is biphasic, and an intermediate state appears to be populated at about 2 M GdnHCl/urea. The transition midpoints defined by horizontal baselines and the plateau are at 0.9 M for the first phase and at 2.7 M GdnHCl for the second phase. Data beyond 4 M denaturant concentrations exhibit a posttransition slope without any other obvious transitions and, hence, are not shown here.

We were interested to determine whether Sml1p could be reversibly unfolded and refolded. Refolding of Sml1p was measured by first treating the protein with high concentrations of GdnHCl (final 4.8 M) for 12 h, and then allowing refolding to proceed by diluting 10-fold in varying mixtures of denaturant and buffer over a period of 24 h. The refolding behavior exhibited both by WT and C14S Sml1p treated with GdnHCl is plotted (with open symbols) in Figure 5A. Because the unfolding and refolding curves superimpose well, this suggests that the chemical unfolding of Sml1p is a reversible process.

To further probe the unfolding of Sml1p, we conducted experiments that examined the concentration dependence of unfolding. Figure 6A displays the concentration dependence of WT Sml1p denaturation, and Figure 6B shows C14S Sml1p denaturation. No significant change in the transition profiles is observed over a 10-fold difference in protein concentration for both WT and C14S Sml1p. The lack of concentration dependence in the unfolding behavior indicates that the protein remains in its dimeric form, even in a partially unfolded state, at intermediate GdnHCl concentrations. To confirm the integrity of the dimeric structure at these concentrations of denaturant, the oligomeric state of Sml1p (both WT and C14S) in varying concentrations of GdnHCl was analyzed by sedimentation equilibrium using an analytical ultracentrifuge, because this is the most reliable technique

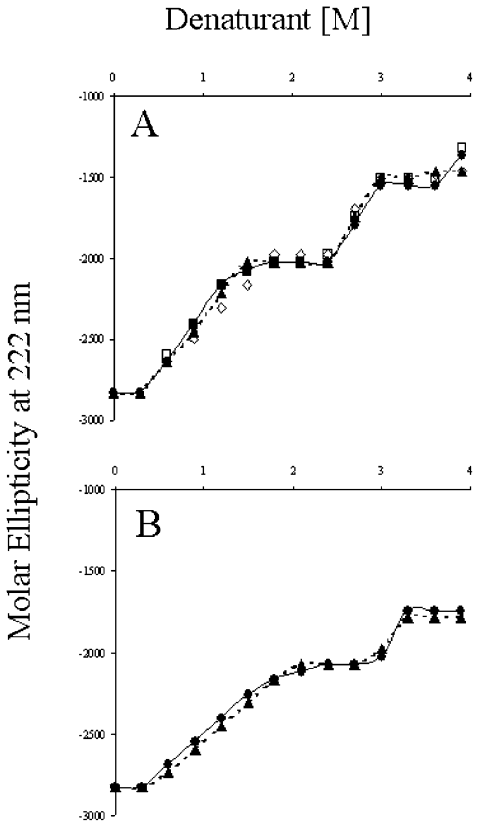

FIGURE 5: Unfolding and refolding curves for WT and C14S Sml1p. Panel A shows a plot of molar ellipticity at 222 nm versus GdnHCl concentration for WT (●) and C14S (▲) Sml1p. Also shown in the figure with open symbols (□ for WT and ◇ for C14S) is reversible refolding from a solution of 4.8 M GdnHCl as described in Materials and Methods. Panel B shows denaturation of both WT (●) and C14S (▲) Sml1p with urea. Smooth lines through the data (solid for WT and dashed for C14S) are for presentation purposes only and do not represent fits to any model.

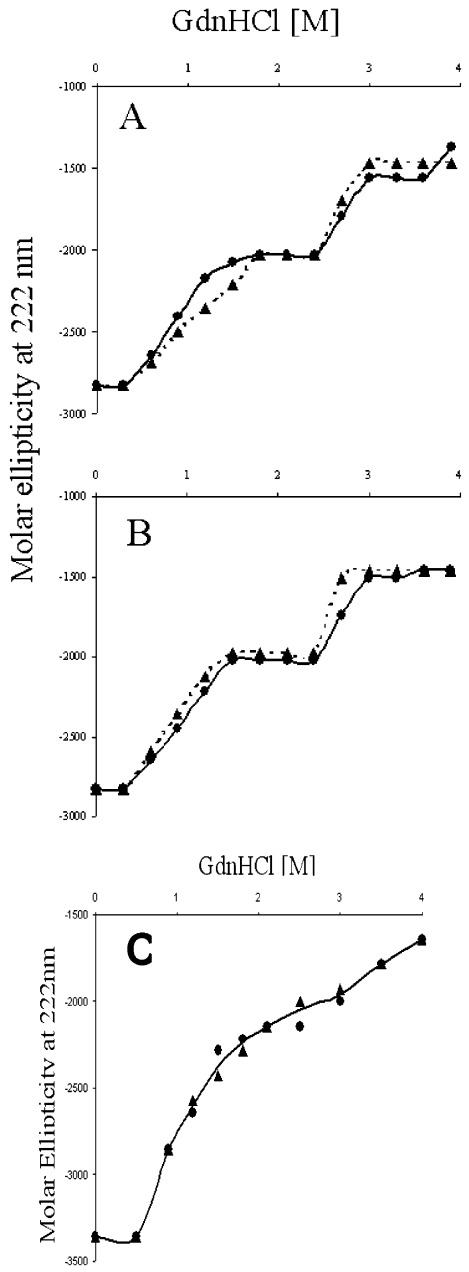

FIGURE 6: Concentration-independent unfolding curves for WT, C14S, and Δ38Sml1p. Panel A shows unfolding of 2 (●) and 20 μM (▲) WT Sml1p in GdnHCl, whereas panel B shows unfolding of 2 (●) and 20 μM (▲) C14S Sml1p in GdnHCl. Smooth lines through the data (solid for 2 μM and dashed for 20 μM) are for presentation purposes only and do not represent fits to any model. Panel C shows the unfolding of 2 (●) and 20 μM (▲) Δ38Sml1p in GdnHCl. The smooth line drawn through the data is for presentation purposes only and does not represent fits to any model.

for determining molecular weight in a shape-independent manner. These results confirmed that even at 4.8 M GdnHCl the Sml1p dimer does not dissociate to form monomers. Dissociation to a monomer is only observed at the highest (7.3 M) GdnHCl concentrations. The data for C14S Sml1p denatured in 7.3 M GdnHCl (Figure 7) fit to a single species of molecular weight corresponding to 11 200 Da.

In light of the observation that Δ38Sml1p is a monomer, it was logical to follow its denaturation by chaotropes for comparison with that of the intact dimer. Figure 6C shows the unfolding of Δ38Sml1p at two different protein concentrations. In contrast to the denaturation behavior of the intact dimer, the truncated protein exhibits only a single broad unfolding transition. The measured unfolding is independent of protein concentration, as expected for a monomer.

Sml1p does not exhibit significant sequence similarity with any protein of known structure in the PDB from queries using a sequence−sequence search technique, like PSI-BLAST (*46*). The secondary structure prediction program PSIPRED predicted four α-helices from residues 6−18, 22−32, 59−76, and 88−95 (Figure 8A). Two predicted helical regions are in agreement with the NMR data (*23*). This secondary structure data was used in the threading program PROSPECT.

None of the predictions by the three fold-recognition programs give high confidence values, suggesting that Sml1p might have a novel structural fold. Hence we have applied the Rosetta/I-sites approach, which is more applicable to novel protein structure predictions (*53*). The top five models for Sml1p have an α-helix from 60 to 76, which is in agreement with the NMR data and secondary structure prediction (ref *23* and Figure 8B). The only difference among these models is that some have a random coil in the 28 C-terminal residues whereas others have an extra α-helical segment. This result is interesting since NMR data showed that the C-terminus of free Sml1p is a random coil structure. It is possible that upon binding to Rnr1p, the unstructured

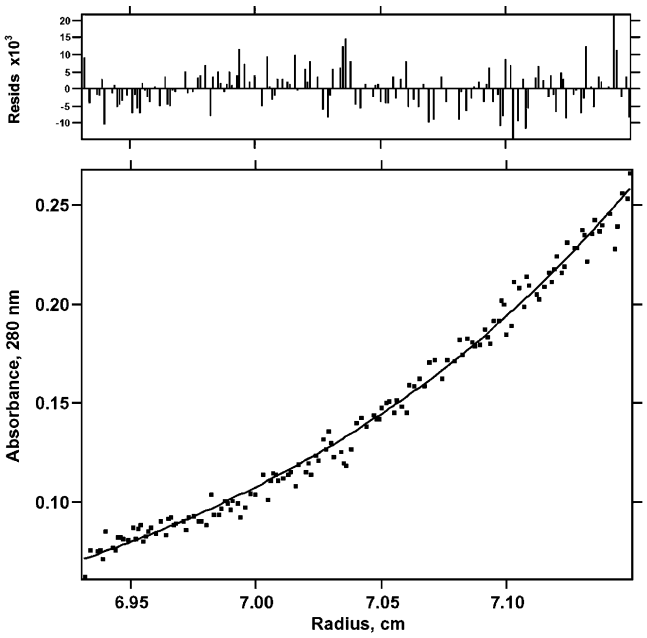

FIGURE 7: Equilibrium analytical centrifugation of C14S Sml1p under denaturing conditions. This figure shows the radial distribution of absorbance in the centrifuge cell after reaching equilibrium with a centrifugation speed of 30 000 rpm for C14S Sml1p (0.2 mg/mL) in 7.3 M GdnHCl. The solid line through the data represents the best fit to a single species model, yielding a molecular weight of 11 200 Da. Residuals for the fit are shown in the upper panel.

C-terminus of Sml1p will change conformation to become α-helical. Figure 8B shows the model of Sml1p with predicted N-terminal and C-terminal helices that are in agreement with the NMR data (*23*). To evaluate the stereochemistry of this model, the Ramachandran plot (inset to Figure 8B) was created using PROCHECK. The plot shows that over 90% of the residues are in the most favored regions, and none of the residues are in disallowed regions.

We feel confident about the overall structural fold of the predicted model for the following reasons: (1) the top ranked model by the program Rosetta has a reasonably high confidence score; (2) the model is consistent with known experimental and predicted secondary structure; (3) the model is of very high quality as evaluated by Ramachandran plot. Our experience suggests that an incorrectly predicted structural fold with such a good Ramachandran plot is extremely rare.

DISCUSSION

The sedimentation equilibrium analytical ultracentrifugation experiments were used as the main method to determine the oligomeric state of WT and C14S Sml1p. Previously, protein purification using gel filtration chromatography for both WT and C14S Sml1p conducted under reducing and nonreducing conditions, respectively, showed a retention volume characterized by a single sharp and symmetrical peak corresponding to molecular mass of 23 kDa. This result was noteworthy because previously we had identified a Sml1p dimer that was linked by a disulfide bond (*24*), whereas this indicated that Sml1p remained a dimer, even in the absence of an intermolecular disulfide. Because size-exclusion chromatography is influenced by the shape of a protein, we resorted to sedimentation equilibrium ultracentrifugation analysis to give us an accurate shape-independent molecular weight of Sml1p. The shape independence of the method can be observed by examining eq 2, which expresses the molecular weight *M* independent of a shape function (*37*). The sedimentation equilibrium experiments show that Sml1p is a homogeneous sample as indicated by the presence of a single-exponential distribution in the cell (Figure 2). Fitting independent data sets at different protein concentrations and rotor speeds to a single species model gives a molecular weight in agreement with the molecular mass for a dimer. Sedimentation equilibrium experiments performed under reducing as well as nonreducing conditions showed that both WT and C14S Sml1p exist as dimers over a series of concentrations that extend from 20 to 100 μM range (Table 1). Moreover, Sml1p exists as a dimer at both 4 and 30 °C, the physiologic temperature of *S. cerevisiae*. These results suggest that dimerization is independent of intermolecular disulfide bonding.

We have localized the region responsible for dimerization to the N-terminal 8−20 amino acids after subjecting a set of N-terminal truncation mutants to sedimentation equilibrium studies (see Table 2). These residues consist of a mixture of two charged, two hydrophobic, and six polar residues. A careful examination of the molecular model of Sml1p (see Figure 8) shows residues 6−18 in a helical conformation. We know that helices can be involved in protein−protein interactions.

The overall unfolding pathway for a dimeric protein like Sml1p must begin with the folded dimer (N_2) and end with two unfolded monomers (2U). The way in which this process occurs depends on whether intermediates involving dissociated monomers (2M) are present along the pathway. Numerous examples exist for both compact monomeric or dimeric intermediates that are significantly populated during the equilibrium denaturation of a folded dimer (41−42). In this work, we have carried out unfolding/refolding studies of Sml1p variants to distinguish between the two mechanisms of unfolding. The unfolding of Sml1p as a function of secondary structure was monitored by CD over a range of denaturant concentrations using both GdnHCl and urea. In general, unfolding of the protein secondary structure by GdnHCl gives insights to the stabilizing contributions made by hydrophobic/nonionic interactions only, whereas, stabilization of the secondary structure by electrostatic and hydrophobic/nonionic intramolecular interactions can be monitored by using urea as the chaotropic agent (*38*). The transition midpoints for both WT and C14S are in the same range for both denaturants (Figure 5), suggesting that hydrophobic interactions are strongly involved in stabilizing secondary structural components of Sml1p. Furthermore, for both WT and C14S Sml1p, the transitions occur at the same concentrations of denaturant, indicating that there are no significant energy/stability differences between the WT and the mutant Sml1p.

The unfolding profile of Sml1p over a range up to 4 M GdnHCl concentrations clearly shows two reversible transitions with midpoints at 0.9 and 2.7 M denaturant. A simple three-state model that could describe these two intermediates would be $N_2 \leftrightarrow 2M \leftrightarrow 2U$ where N_2 is folded dimer, M is a folded monomer, and U is an unfolded monomer. If dimeric Sml1p were to dissociate during the first transition, $N_2 \leftrightarrow 2M$, this process should be concentration-dependent. The

A

```
Conf: 9876201244432223314402322205674037888533454311222346644433 02
Pred: CCCCCHHHHHHHHHHHHHCCCHHHHHHHHHHHCCCCCCCCCCCCCCCCCCCCCCCCHH
  AA: MQNSQDYFYAQNRCQQQQAPSTLRTVTMAEFRRVPLPPMAEVPMLSTQNSMGSSASASAS
              10        20        30        40        50        60

Conf: 3577889999987552033346754642577654215542257 9
Pred: HHHHHHHHHHHHHHHHCCCCCCCCCCCCHHHHHHHHCCCCCCCCC
  AA: SLEMWEKDLEERLNSIDHDMNNNKFGSGELKSMFNQGKVEEMDF
              70        80        90       100
```

B

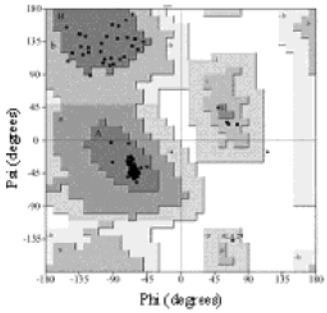

FIGURE 8: Three-dimensional molecular model of Sml1p. Panel A shows the secondary structure prediction of Sml1p by PSIPRED. Four α-helices (6−18, 22−32, 59−76, and 88−95) were predicted by PSIPRED. Conf denotes confidence (0 = low, 9 = high); pred denotes predicted secondary structure (H = helix, E = strand, C = coil). Panel B shows the 3-dimensional model of Sml1p; N = N-terminus, and C = C-terminus. Ramachandran plot shown as an inset to panel B was created by the PROCHECK program; 85 residues out of 104 (91.4%) are in the most favored regions, and none of the residues are in the disallowed regions.

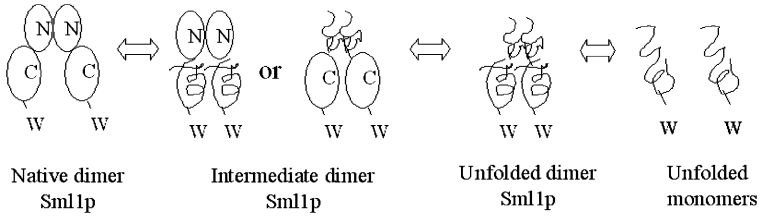

FIGURE 9: Minimal model for unfolding of Sml1p. In this model, native dimer when perturbed initially by increasing GdnHCl concentration induces first unfolding of the unstable domain (it may be either of N or C terminal domain) followed by subsequent unfolding of the stable domain. Upon increasing the GdnHCl concentration to ~7.3 M, the unfolded dimer dissociates into unfolded monomers.

second transition, M ↔ U, is unimolecular and should be independent of protein concentration. Our tests of concentration dependence contradict this model because Sml1p concentrations varied over a 10-fold range show the same profile for both transitions (Figure 6), indicating that there are no association or dissociation phenomena that accompany unfolding of the protein. To confirm that the Sml1p dimer does not dissociate to two monomers at concentrations of GdnHCl associated with the second transition, we conducted analytical ultracentrifugation of Sml1p between 1.8 and 7.3 M denaturant concentrations (Table 3). The results from these experiments show that Sml1p exists as a dimer at GdnHCl concentrations up to 6.5 M but ultimately dissociates at 7.3 M GdnHCl. The sedimentation equilibrium data also rules out the possibility of a Sml1p monomer that has two domains independently undergoing unfolding for the reasons stated above.

Alternatively, the two transitions are interpreted in terms of unfolding of two separate domains as a function of GdnHCl treatment. In our case, a minimal model that accounts for all experimental observations is $N_2 \leftrightarrow I_1 \leftrightarrow I_2 \leftrightarrow 2U$, where N_2 is the native dimer, I_1 and I_2 are two distinct dimeric intermediates corresponding to independently unfolded domains, and U is the unfolded monomer. The cartoon diagram representing this model is shown in Figure 9. In

Table 3: Results of Molecular Weight Determined by Equilibrium Analytical Centrifugation of WT and Mutant Variants of Sml1p at a Concentration of 0.8 mg/mL in 20 mM Tris (pH 7.5), 120 mM NaCl, 5 mM $MgCl_2$, and 5 mM DTT Containing Varying Concentrations from 1.8 to 7.3 M GdnHCl

protein	conc of GdnHCl (M)	MW[a]	χ^2
C14SSml1p	1.8	25 600	0.006
C14SSml1p	3.3	27 400	0.002
C14SSml1p	4.2	30 000	0.002
C14SSml1p	4.8	29 000	0.01
C14SSml1p	5.5	25 700	0.054
C14SSml1p	6.5	21 900	0.07
C14SSml1p	7.3	11 200	0.05
WT Sml1p	5.5	26 900	0.1
WT Sml1p	6.5	22 200	0.08

[a] Molecular weights calculated for a single-species fit.

this model, native Sml1p is a dimer, and dimerization is a property of the N-terminal domain. Increasing concentrations of denaturant first unfold a less stable domain, followed by unfolding of a second slightly more stable domain. Only high concentrations of denaturant result in dissociation of unfolded dimer to unfolded monomers. This model is corroborated by the fact that Δ38Sml1p, where most of the Sml1p N-terminus is truncated, has a single unfolding transition (Figure 6C). Several other groups have also observed that partially folded dimeric intermediates exist within an unfolding pathway (39−41). In the case of the domain-swapped dimer reported by Rousseau et al. (*39*), the β4 sheet and the hinge loop region play a critical role in dimerization as well as stabilization of their reported partially folded dimeric intermediate within the folding pathway. In the case of the cystatins, the dimer is observed in the native and molten globule states (*40*). Furthermore, Louzada and co-workers observe a so-called "predissociated" dimer at 2.5 M GdnHCl (*41*). Here the dimer represents a partially folded intermediate. An interesting question that arises out of these observations is what manner of interactions is likely to occur in a protein placed in a solution containing a high chaotropic concentration? Recent reports suggest that there is residual structure at high chaotropic concentrations possibly permitting a limited set of interactions (*41*−*44*). Although in the absence of a crystal structure it is not known whether Sml1p exists as a domain-swapped dimer, similar interactions may play a role in stabilizing the dimeric folding intermediates.

A further assessment of the gross shape and domain organization of Sml1p was obtained using computational methods. Template-based approaches were used to model the three-dimensional structure for this protein (Figure 8B). The molecular model predicts Sml1p to be a loosely folded, two-domain, elongated protein. The function of the two domains are as follows: the C-terminal domain is the Rnr1p binding domain (*23*), and we propose that the N-terminal domain is responsible for dimerization. However, we cannot rule out other functions of the N-terminal domain. For example, a search for PEST sequences (rich in proline, glutamate, serine and threonine) identifies a weak PEST sequence in the region from 33 to 66 in the sequence of Sml1p (Figure 8a). Recently we have identified the residues of Sml1p phosphorylated by Dun1p to be Ser56, Ser58, and Ser60 (*22*). It may be that this region of the protein is a target for ubiquitination to trigger degradation through the cellular machinery (*47*, *48*). Also, the presence of a PXXP motif (residues 35−58 in Figure 8a) may be recognized by SH3 domain containing proteins (*49*−*52*) and further regulate Sml1p activity in the cell.

ACKNOWLEDGMENT

We appreciate Kenneth Minor for helping us with some of the analytical ultracentrifugation experiments. We are very grateful to Dr. Elias J. Fernandez for sharing his modified pGEX vector with us. We also thank Brad Bennett, Sanath Wijerathna, Dr. Cat Faber, and Matt Wilkerson in critical reading and preparation of this manuscript. We acknowledge Dr. George Rose for insightful discussions.

REFERENCES

1. Friedberg, E. C., Bardwell, A. J., Bardwell, L., Feaver, W. J., Kornberg, R. D., Svejstrup, J. Q., Tomkinson, A. E., and Wang, Z. (1995) Nucleotide excision repair in the yeast *Saccharomyces cerevisiae*: its relationship to specialized mitotic recombination and RNA polymerase II basal transcription, *Philos. Trans. R. Soc. London, Ser. B 347*, 63−68.
2. Siede, W., Friedberg, A. S., and Friedberg, E. C. (1993) RAD9-dependent G1 arrest defines a second checkpoint for damaged DNA in the cell cycle of *Saccharomyces cerevisiae*, *Proc. Natl. Acad. Sci. U.S.A. 90*, 7985−7989.
3. Craven, R. J., and Petes, T. D. (2000) Involvement of the checkpoint protein Mec1p in silencing of gene expression at telomeres in *Saccharomyces cerevisiae*, *Mol. Cell. Biol. 20*, 2378−2384.
4. Murnane, J. P. (1995) Cell cycle regulation in response to DNA damage in mammalian cells: a historical perspective, *Cancer Metastasis Rev 14*, 17−29.
5. Fasullo, M., Koudelik, J., AhChing, P., Giallanza, P., and Cera, C. (1999) Radiosensitive and mitotic recombination phenotypes of the *Saccharomyces cerevisiae* dun1 mutant defective in DNA damage-inducible gene expression, *Genetics 152*, 909−919.
6. Machado, A. K., Morgan, B. A., and Merrill, G. F. (1997) Thioredoxin reductase-dependent inhibition of MCB cell cycle box activity in *Saccharomyces cerevisiae*, *J. Biol. Chem. 272*, 17045−17054.
7. Elledge, R. M. (1996) Assessing p53 status in breast cancer prognosis: where should you put the thermometer if you think your p53 is sick? *J. Natl. Cancer Inst. 88*, 141−143.
8. Zhao, X., and Rothstein, R. (2002) The Dun1 checkpoint kinase phosphorylates and regulates the ribonucleotide reductase inhibitor Sml1, *Proc. Natl. Acad. Sci. U.S.A. 99*, 3746−3751.
9. Jordan, A., and Reichard, P. (1998) Ribonucleotide reductases, *Annu. Rev. Biochem. 67*, 71−98.
10. Brown, N. C. a. R. P. (1969) Role of effector binding in allosteric control of ribonucleoside diphosphate reductase, *J. Mol. Biol. 46*, 39−55.
11. Huang, M., and Elledge, S. J. (1997) Identification of RNR4, encoding a second essential small subunit of ribonucleotide reductase in *Saccharomyces cerevisiae*, *Mol. Cell. Biol. 17*, 6105−6113.
12. Elledge, S. J., Zhou, Z., Allen, J. B., and Navas, T. A. (1993) DNA damage and cell cycle regulation of ribonucleotide reductase, *Bioessays 15*, 333−339.
13. Elledge, S. J., and Davis, R. W. (1990) Two genes differentially regulated in the cell cycle and by DNA-damaging agents encode alternative regulatory subunits of ribonucleotide reductase, *Genes Dev. 4*, 740−751.
14. Bjorklund, S., Skog, S., Tribukait, B, and Thelander, L. (1990) S-phase-specific expression of mammalian ribonucleotide reductase R1 and R2 subunit mRNAs, *Biochemistry 29*, 5452−5458.
15. Engstrom, Y., Eriksson, S., Jildevik, I., Skog, S., Thelander, L., and Tribukait, B. (1985) Cell cycle-dependent expression of mammalian ribonucleotide reductase. Differential regulation of the two subunits, *J. Biol. Chem. 260*, 9114−9116.
16. Yao, R., Zhang, Z., An, X., Bucci, B., Perlstein, D. L., Stubbe, J., and Huang, M. (2003) Subcellular localization of yeast ribonucleotide reductase regulated by the DNA replication and damage checkpoint pathways, *Proc. Natl. Acad. Sci. U.S.A. 100*, 6628−6633.
17. Chabes, A., Domkin, V., and Thelander, L. (1999) Yeast Sml1, a protein inhibitor of ribonucleotide reductase, *J. Biol. Chem. 274*, 36679−36683.
18. Vallen, E. A., and Cross, F. R. (1999) Interaction between the MEC1-dependent DNA synthesis checkpoint and G1 cyclin function in *Saccharomyces cerevisiae*, *Genetics 151*, 459−471.
19. Chaboute, M. E., Combettes, B., Clement, B., Gigot, C., and Philipps, G. (1998) Molecular characterization of tobacco ribonucleotide reductase RNR1 and RNR2 cDNAs and cell cycle-regulated expression in synchronized plant cells, *Plant Mol. Biol. 38*, 797−806.
20. Elledge, S. J., Zhou, Z., and Allen, J. B. (1992) Ribonucleotide reductase: regulation, regulation, regulation, *Trends Biochem. Sci. 17*, 119−123.
21. Zhao, X., Chabes, A., Domkin, V., Thelander, L., and Rothstein, R. (2001) The ribonucleotide reductase inhibitor Sml1 is a new target of the Mec1/Rad53 kinase cascade during growth and in response to DNA damage, *EMBO J. 20*, 3544−3553.
22. Uchiki, T., Dice, L. T., Hettich, R. L., and Dealwis, C. (2004) Identification of phosphorylation sites on the yeast ribonucleotide reductase inhibitor Sml1, *J. Biol. Chem. 279*, 11293−11303.

23. Zhao, X., Georgieva, B., Chabes, A., Domkin, V., Ippel, J. H., Schleucher, J., Wijmenga, S., Thelander, L., and Rothstein, R. (2000) Mutational and structural analyses of the ribonucleotide reductase inhibitor Sml1 define its Rnr1 interaction domain whose inactivation allows suppression of mec1 and rad53 lethality, *Mol. Cell. Biol. 20*, 9076−9083.
24. Uchiki, T., Hettich, R., Gupta, V., and Dealwis, C. (2002) Characterization of monomeric and dimeric forms of recombinant Sml1p-histag protein by electrospray mass spectrometry, *Anal. Biochem. 301*, 35−48.
25. Knott, J. A., Orr, D. C., Montgomery, D. S., Sullivan, C. A., and Weston, A. (1989) The expression and purification of human rhinovirus protease 3C, *Eur. J. Biochem. 182*, 547−555.
26. Minor, K. H., and Peterson, C. B. (2002) Plasminogen activator inhibitor type 1 promotes the self-association of vitronectin into complexes exhibiting altered incorporation into the extracellular matrix, *J. Biol. Chem. 277*, 10337−10345.
27. Kawahara, K., and Tanford, C. (1966) Viscosity and density of aqueous solutions of urea and guanidine hydrochloride, *J. Biol. Chem. 241*, 3228−3232.
28. Vistica, J., Dam, J., Balbo, A., Yikilmaz, E., Mariuzza, R. A., Rouault, T. A., and Schuck, P. (2004) Sedimentation equilibrium analysis of protein interactions with global implicit mass conservation constraints and systematic noise decomposition, *Anal. Biochem.*, in press.
29. McGuffin, L. J., Bryson, K., and Jones, D. T. (2000) The PSIPRED protein structure prediction server, *Bioinformatics 16*, 404−405.
30. Xu, Y., and Xu, D. (2000) Protein threading using PROSPECT: design and evaluation, *Proteins 40*, 343−354.
31. Jones, D. T. (1999) GenTHREADER: an efficient and reliable protein fold recognition method for genomic sequences, *J. Mol. Biol. 287*, 797−815.
32. Bar, G., Bennati, M., Nguyen, H. H., Ge, J., Stubbe, J. A., and Griffin, R. G. (2001) High-frequency (140-GHz) time domain EPR and ENDOR spectroscopy: the tyrosyl radical-diiron cofactor in ribonucleotide reductase from yeast, *J. Am. Chem. Soc. 123*, 3569−3576.
33. Bystroff, C., Thorsson, V., and Baker, D. (2000) HMMSTR: a hidden Markov model for local sequence-structure correlations in proteins, *J. Mol. Biol. 301*, 173−190.
34. Sali, A., and Overington, J. P. (1994) Derivation of rules for comparative protein modeling from a database of protein structure alignments, *Protein Sci. 3*, 1582−1596.
35. Laskowski, R. A., MacArthur, M. W., Moss, D. M., and Thornton, J. M. (1993) *PROCHECK*: a program to check the stereochemical quality of protein structures, *Appl. Crystallogr. 26*, 283−290.
36. Sayle, R. A., and Milner-White, E. J. (1995) RASMOL: biomolecular graphics for all, *Trends Biochem. Sci. 20*, 374.
37. Schachman, H. K. (1959) *Ultracentrifugation in Biochemistry*, Academic Press, New York.
38. Monera, O. D., Kay, C. M., and Hodges, R. S. (1994) Protein denaturation with guanidine hydrochloride or urea provides a different estimate of stability depending on the contributions of electrostatic interactions, *Protein Sci. 3*, 1984−1991.
39. Rousseau, F., Schymkowitz, J. W., Wilkinson, H. R., and Itzhaki, L. S. (2004) Intermediates control domain swapping during folding of p13suc1, *J. Biol. Chem. 279*, 8368−8377.
40. Staniforth, R. A., Giannini, S., Higgins, L. D., Conroy, M. J., Hounslow, A. M., Jerala, R., Craven, C. J., and Waltho, J. P. (2001) Three-dimensional domain swapping in the folded and molten-globule states of cystatins, an amyloid-forming structural superfamily, *EMBO J. 20*, 4774−4781.
41. Louzada, P. R., Sebollela, A., Scaramello, M. E., and Ferreira, S. T. (2003) Predissociated dimers and molten globule monomers in the equilibrium unfolding of yeast glutathione reductase. *Biophys. J. 85*, 3255−3261.
42. Shortle, D., and Ackerman, M. S. (2001) Persistence of nativelike topology in a denatured protein in 8 M urea, *Science 293*, 487−489.
43. Kazmirski, S. L., Wong, K. B., Freund, S. M., Tan, Y. J., Fersht, A. R., and Daggett, V. (2001) Protein folding from a highly disordered denatured state: the folding pathway of chymotrypsin inhibitor 2 at atomic resolution, *Proc. Natl. Acad. Sci. U.S.A. 98*, 4349−4354.
44. Sanchez, I. E. a. K. T. (2003) Origin of Unusual f-values in protein folding: evidence against specific nucleation sites, *J. Mol. Biol. 334*, 1077−1085.
45. Zhao, X., Muller, E. G. D., and Rothstein, R. (1998) A suppressor of two essential checkpoint genes identifies a novel protein that negatively affects dNTP pools, *Mol. Cell 2*, 329−340.
46. Altschul, S. F., and Koonin, E. V. (1998) Iterated profile searches with PSI-BLAST−a tool for discovery in protein databases, *Trends Biochem. Sci. 23*, 444−447.
47. Rechsteiner, M., and Rodgers, S. W. (1996) PEST sequences and regulation by proteolysis, *Trends Biochem. Sci. 21*, 267−271.
48. Hochstrasser, M. (1996) Ubiquitin-dependent protein degradation, *Annu. Rev. Genet. 30*, 405−439.
49. Cicchetti, P., Mayer, B. J., Thiel, G., and Baltimore, D. (1992) Identification of a protein that binds to the SH3 region of Abl and is similar to Bcr and GAP-rho, *Science 257*, 803−806.
50. Gout, I., Dhand, R., Hiles, I. D., Fry, M. J., Panayoutou, G., Das, P., Truong, O., Totty, N. F., Hsuan, J., Booker, G. W., Campbell, I. D., and Waterfield, M. D. (1993) The GTPase dynamin binds to and is activated by a subset of SH3 domains, *Cell 75*, 25−36.
51. Buday, L., and Downward, J. (1993) Epidermal growth factor regulates p21ras through the formation of a complex of receptor, Grb2 adaptor protein and Sos nucleotide exchange factor, *Cell 73*, 610-620.
52. Ren, R., Mayer, B. J., Cicchetti, P., and Baltimore, D. (1993) Identification of a ten-amino acid proline-rich SH3 binding site, *Science 259*, 1157−1161.
53. Bystroff, C., and Shao, Y. (2002) Fully automated ab initio protein structure prediction using I-SITES, HMMSTR, and ROSETTA, *Bioinformatics 18*, S54−S61.

BI0361721